Monocytes use protrusive forces to generate migration paths in viscoelastic collagen-based extracellular matrices

Author list: Kolade Adebowale[1,2,3], Byunghang Ha[4,] Aashrith Saraswathibhatla[4], Dhiraj Indana[4], Medeea C. Popescu[5], Sally Demirdjian[5], Jin Yang[6], Michael C. Bassik[7], Christian Franck[8], Paul L. Bollyky[5], Ovijit Chaudhuri[2,4*]

[1]Department of Chemical Engineering, Stanford University, Stanford, CA, USA 94305
[2]Chemistry, Engineering, and Medicine for Human Health (ChEM-H) Stanford University, Stanford, CA, USA 94305
[3]John A. Paulson School of Engineering and Applied Sciences, Harvard University, Cambridge, MA, USA 02134
[4]Department of Mechanical Engineering, Stanford University, Stanford, CA, USA 94305
[5]Department of Infectious Diseases, Stanford University, Stanford, CA, USA 94305
[6]Department of Aerospace Engineering and Engineering Mechanics, University of Texas at Austin, Austin, TX USA 78712
[7]Department of Genetics, Stanford University, Stanford, CA, USA 94305
[8]Department of Mechanical Engineering, University of Wisconsin-Madison, Madison, WI USA 53706

***Corresponding author:** Ovijit Chaudhuri
***Email:** chaudhuri@stanford.edu

Author Contributions: K.A., P.L.B, and O.C. designed the experiments. K.A. performed rheometry, substrate preparation, time-lapse microscopy cell migration experiments, performed experimental data analysis, and statistical tests. B.H. performed cell migration experiments for matrix displacement analysis, and A.S. and J.Y. performed matrix displacement data analysis. D.I. performed immunohistochemical staining. M.P. and S.D. extracted primary human cells. R.K. and M.C.B contributed to CRISPR knockout studies. K.A., C.F., P.L.B, and O.C. wrote the manuscript.

Competing Interests Statement:
The authors declare no competing financial interests.

Classification: Physical Sciences (Biophysics) and Biological Sciences (Cell Biology)

Keywords: monocytes, migration, stromal matrix, viscoelasticity

This PDF file includes:

Main Text
Figures 1 to 5

Abstract

Circulating monocytes are recruited to the tumor microenvironment, where they can differentiate into macrophages that mediate tumor progression. To reach the tumor microenvironment, monocytes must first extravasate and migrate through the type-1 collagen rich stromal matrix. The viscoelastic stromal matrix around tumors not only stiffens relative to normal stromal matrix, but often exhibits enhanced viscous characteristics, as indicated by a higher loss tangent or faster stress relaxation rate. Here, we studied how changes in matrix stiffness and viscoelasticity, impact the three-dimensional migration of monocytes through stromal-like matrices. Interpenetrating networks of type-1 collagen and alginate, which enable independent tunability of stiffness and stress relaxation over physiologically relevant ranges, were used as confining matrices for three-dimensional culture of monocytes. Increased stiffness and faster stress relaxation independently enhanced the 3D migration of monocytes. Migrating monocytes have an ellipsoidal or rounded wedge-like morphology, reminiscent of amoeboid migration, with accumulation of actin at the trailing edge. Matrix adhesions and Rho-mediated contractility were dispensable for monocyte migration in 3D, but migration did require actin polymerization and myosin contractility. Mechanistic studies indicate that actin polymerization at the leading edge generates protrusive forces that open a path for the monocytes to migrate through in the confining viscoelastic matrices. Taken together, our findings implicate matrix stiffness and stress relaxation as key mediators of monocyte migration and reveal how monocytes use pushing forces at the leading edge mediated by actin polymerization to generate migration paths in confining viscoelastic matrices.

Significance Statement

Cell migration is essential for numerous biological processes in health and disease, including for immune cell trafficking. Monocyte immune cells migrate through extracellular matrix to the tumor microenvironment where they can play a role in regulating cancer progression. Increased extracellular matrix (ECM) stiffness and viscoelasticity have been implicated in cancer progression, but the impact of these changes in the ECM on monocyte migration remains unknown. Here, we find that increased ECM stiffness and viscoelasticity promote monocyte migration. Interestingly, we reveal a previously undescribed adhesion-independent mode of migration whereby monocytes generate a path to migrate through pushing forces at the leading edge. These findings help elucidate how changes in the tumor microenvironment impact monocyte trafficking and thereby disease progression.

Main Text

Introduction

Immune cell migration plays an important role during inflammation and cancer progression(1, 2). Monocytes, a subset of immune cells, are disproportionately recruited from the blood stream during these processes, and they migrate through the extracellular matrix (ECM) to reach the tumor where they differentiate into macrophages(3). Cancer progression is often associated with changes in the mechanical properties of the viscoelastic ECM, suggesting that the impact of these changes on monocyte migration could be significant to cancer progression. Specifically, mechanical properties of the ECM

such as stiffness, viscoelasticity, and collagen fiber architecture, are altered during malignancy for certain cancers. For example, in breast cancer, stiffness increases from ~0.1 – 1 kPa in normal tissues to ~1 – 10 kPa for in malignant tumors(4-7). In addition, some tumors exhibit greater viscous-like behavior compared to normal tissues(4, 8, 9). In biological tissues and ECMs, the viscous resistance, as measured by the loss modulus, is typically around 10% of the elastic resistance, as measured by the storage modulus, at 1 Hz, thus exhibiting a loss tangent of 0.1(10). One consequence of this viscoelastic behavior is that the resistance of the matrix to deformation is reduced over time, a behavior termed stress relaxation. The characteristic timescales of stress relaxation in tissues can range from greater than 1,000 seconds to tens of seconds(10). Lastly, the architecture of the collagen-rich, stromal matrix surrounding tumors changes from wavy to linearized architecture(11). The impact of these changes in matrix mechanics on the three-dimensional migration of monocytes remains unknown.

Cell migration is typically characterized as either amoeboid or mesenchymal based on cell morphological characteristics and activity of cytoskeletal and adhesive machinery(12). Amoeboid migration is characterized by rounded or ellipsoidal cell morphologies, weak cell-ECM adhesions, low proteolytic activity, and Rho-mediated contractility(12). Rho-mediated contractility, acting through Rho kinase (ROCK), is thought to be critical for squeezing the nucleus through confining pores, and prior studies have shown that some immune cells, including T-cells, dendritic cells, and neutrophils are capable of integrin-independent motility(13-15). On the other hand, mesenchymal migration involves more elongated cell morphologies, requires strong adhesions, high proteolytic activity, and can be independent of ROCK activity(12). Furthermore, mesenchymal migration, and to a lesser extent amoeboid migration, can require generation of contractile traction forces on the substrate(16-20). While macrophages and neutrophils exhibit both amoeboid and mesenchymal migration characteristics, the morphologies monocytes utilize to migrate remain unclear(2, 21). Furthermore, much of our current understanding of cell migration is based on cell migration on 2D surfaces or in micropatterned confined environments where a migration path is pre-existing. In contrast, immune cell migration in vivo occurs in a three-dimensional context, and migration paths do not always exist.

Here, we investigated the impact of changes in matrix stiffness and viscoelasticity on the three-dimensional migration of monocytes, and how monocytes generate paths to migrate in confining matrices. Interpenetrating networks of alginate and type-1 collagen (IPN) with independently tunable stiffness and stress relaxation are developed to model the type-1 collagen rich stromal matrix. Enhanced stiffness and faster stress relaxation both promote the migration of monocytes. Monocytes migrated using a wedge or ellipsoid morphology and depended on actin polymerization and myosin II activation, but not Rho-mediated contractility. Cells also migrated when encapsulated in non-adhesive viscoelastic matrix consisting of alginate alone with similar characteristics, indicating the dispensability of adhesion for migration under non-adhesive conditions. Mechanistically, cells migrated by generating propulsive forces at the leading edge of the cell, pushing of the trailing edge, which open a migration path in the confining matrix. Together, these results establish matrix viscoelasticity as a key regulator of monocyte cell migration and reveal how monocytes generate paths to migrate in cells in confining matrices.

Results

Development of stromal-like matrices with independently tunable stiffness and viscoelasticity

We developed interpenetrating networks of type-1 collagen and unmodified alginate (IPNs) with independently tunable stiffness and viscoelasticity as a model of the stromal matrix(22). The type-1 collagen network mimics the collagen structure found in the type-1 collagen rich stroma, while the alginate network enables tunability of the overall IPN mechanical properties (Fig. 1A, B). Alginate does not provide any adhesion motifs for cells to bind to and is not susceptible to degradation by mammalian proteases(23). IPN stiffness was increased from 1 kPa to ~2.5 kPa by increasing the amount of calcium crosslinker added by ~50% (Figs. 1C,D). Matrix stress relaxation was modulated from ~100 s (fast relaxing) to ~1,000s (slow relaxing), corresponding to a loss tangent of ~0.12 and ~0.08 respectively, by utilizing high or low molecular weight alginate respectively (Figs. 1E,F. Fig. S1). Note that the strategy to modulate viscoelasticity used here is different from a previous approach with collagen-alginate IPNs that used covalent versus ionic crosslinks where the alginate was chemically modified with norbornene and tetrazine groups to facilitate click chemistry(24). The range of stiffness and stress relaxation developed is relevant to what is observed during breast cancer, pancreatic cancer, and bladder cancer progression(4, 9, 25). The collagen structure, visualized via confocal reflectance microscopy, showed a fiber architecture with micron-scale spacing between fibers (Fig. 1G). The nanoporous alginate mesh is expected to fill the space between the fibers, making these matrices highly confining. Collagen fiber length and width measurements revealed only some minor differences that are not expected to be biologically meaningful (Figs. 1H-K). Taken together, these data demonstrate the development of collagen-alginate IPNs with tunable stiffness and viscoelastic properties with similar collagen fiber architectures.

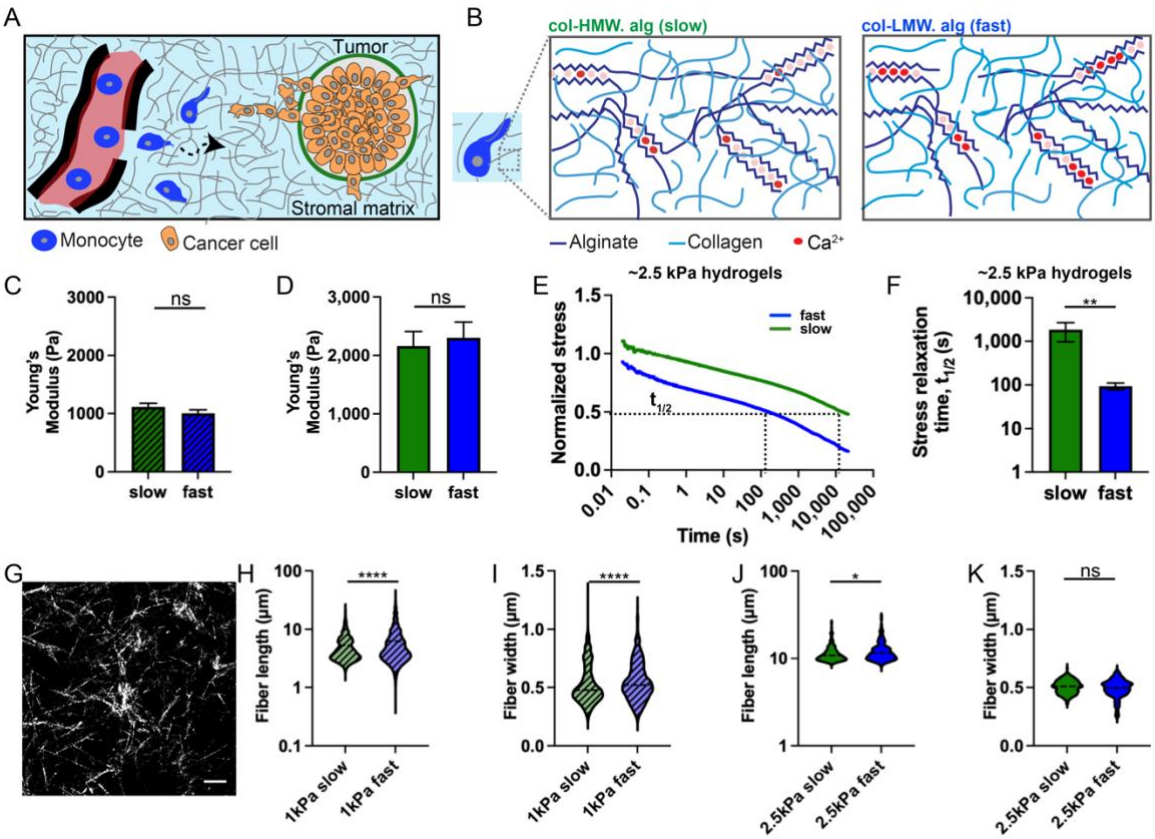

Fig. 1 Interpenetrating networks (IPNs) of alginate and collagen with independently tunable properties are used to model the type-1 collagen rich stromal matrix around tumors. (A) Schematic describing how monocytes recruited from the blood migrate through stromal matrix to reach the tumor microenvironment. (B) Schematic of cell encapsulated in IPN made from high molecular weight (HMW) alginate (slow) and low molecular weight (LMW) alginate (fast). (C,D) Young's modulus measurements of the different IPN formulations d, N = 4 biological replicates for slow and fast. Unpaired t-test; ns p=0.2544, p=0.7130. (E) Representative stress relaxation curves for slow and fast IPNs. (F) Timescale over which the stress relaxes to half its original value for slow and fast relaxing IPNs. N = 4 and 5 for slow and fast respectively. Unpaired t-test; **p=0.0100. (G) Confocal reflectance microscopy of collagen fiber images for IPN. Scale bar: 20 μm. (H-K) Fiber length and width for indicated IPN formulations. N = 2 biological replicates for all conditions. Kolmogorov-Smirnov (due to non-normal distributions); ****p<0.0001, *p=0.0254, ns p = 0.4098. Figs. 1A,B were adapted from previous work(23, 26).

Increased stiffness and faster stress relaxation promote monocyte migration

With the independently tunable collagen-alginate IPNs, we examined the impact of increased stiffness and faster stress relaxation, independently, on monocyte migration. U937 human monocytes or primary human monocytes were encapsulated in 3D matrices and tracked during time-lapse microscopy experiments (Fig. 2A). Monocytes were generally rounded, but more elongated in the fast relaxing IPNs compared to slow relaxing IPNs (Fig. 2B). Cell migration speed, mean squared displacement (MSD), and ratio of cell displacement to cell track length (directionality) were used as quantitative descriptors of migration. Increased stress relaxation or stiffness induced longer cell tracks (Figs. 2C-F). Faster matrix stress relaxation increases cell migration speed for the same stiffness values for U937 cells and primary cells from human patients (Figs. 2G-I, Fig. S2). Cells also migrated with greater speed in stiffer matrices for both slow and fast

relaxing IPNs (Fig. 2J-L). Both the slope and y-intercept of the MSD curve increased with stiffness, indicating that cells migrate more efficiently and with higher free diffusivity as IPN stress relaxation became faster (Fig. 2I). Similar observations were made with increase in matrix stiffness leading to more efficient migrating in fast relaxing IPN (Fig. 2L). Taken together, these results demonstrate that faster matrix stress relaxation and increased stiffness both promote increased migration in monocytes.

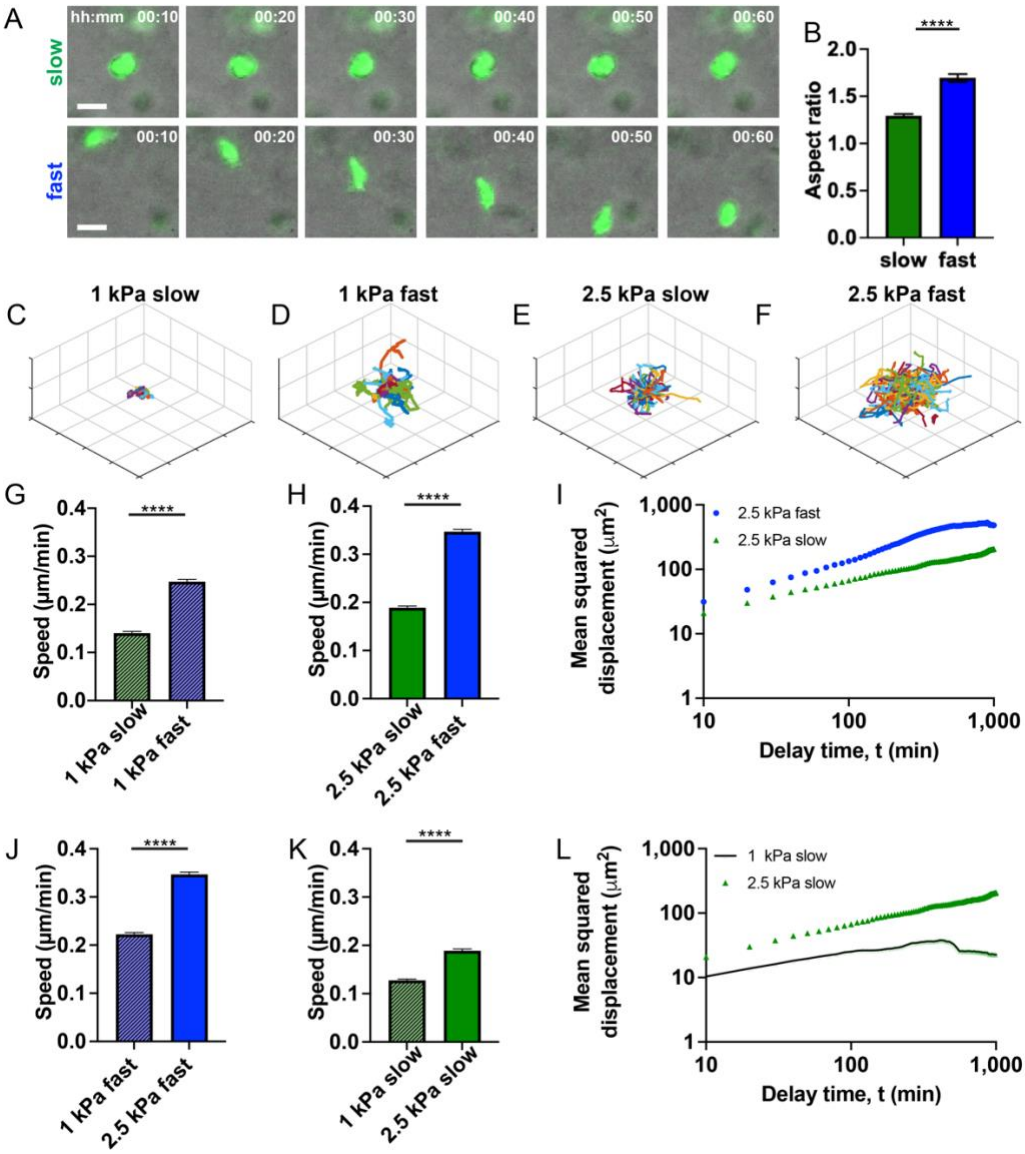

Fig. 2 Faster stress relaxation and increased stiffness independently promote enhanced three-dimensional migration of monocytes. (A) Representative images of cells embedded in slow relaxing (top row) and fast relaxing (bottom row) hydrogels. Scale bar: 20 μm. (B) Aspect ratio of monocytes embedded in slow or fast relaxing matrix. n = 132 cells and N = 2 biological replicates. (C-F) Representative migration tracks for each of the indicated matrix parameters. Each grid is 50 μm. n > 85 for each condition; N = 1 biological replicate. (G-I)**,** Migration speed, and MSD when stress relaxation is enhanced in 1 kPa or 2.5 kPa gels. (G,H), n > 1,148 for each condition; N = 2 biological replicates. (J-L)**,** Migration speed, and MSD when stiffness (Young's modulus) is increased in slow or fast relaxing gels. (J,K) n > 2,288 for each condition; N = 2 biological replicates. (I,L) n > 116; N = 1 biological replicate. (B,G,H,J,K) Kolmogorov-Smirnov: **** p < 0.0001.

Migrating monocytes are amoeboid-like, migrate independent of matrix adhesions

We examined cell morphology and the potential role of matrix adhesions to determine the mode of migration. Visualization of cells encapsulated in slow and fast relaxing IPNs revealed that the cells were generally rounded or ellipsoidal, suggesting an amoeboid type of migration (Fig 2A). There was dependence on matrix stress relaxation as the ellipsoidal shape of cells in fast relaxing IPNs was marked by a higher aspect ratio and lower circularity compared to cells in slow relaxing IPNs (Figs. 2B, S3). Importantly, cells did not display invasive protrusions (i.e., invadopodia, pseudopodia, filopodia, lobopodia) or blebbing morphologies, which are characteristic of certain kinds of mesenchymal and amoeboid migration.

Cell-matrix adhesions are thought to be important for migration of many cells and critical for mesenchymal migration, though some immune cells are known to be capable of migration independent of adhesions(27). Pharmacological inhibition and CRISPR knockouts (KOs) were applied to perturb the activity of adhesion receptors and associated proteins. Small molecule inhibition of the receptor tyrosine kinase activated in response to collagen, discoidin domain receptor 1 (DDR1), only had a modest impact on cell migration or MSD (Figs. 3A-C). Furthermore, it is thought that monocytes recruited to solid tissues polarize to macrophages whose migration is dependent on heterodimeric $\alpha_M\beta_2$-integrins(2, 28). Interestingly, CRISPR knockout of β_2-integrins resulted in a slight increase in cell migration consistent with what has been observed for human neutrophil migration under confinement(15). But CRISPR knockout of α_M or talin-1, an integrin associated protein, did lead to a decrease in cell migration (Figs. 3A-C). CRISPR KO of β_2-integrins combined with antibody blocking of β_1-integrins only resulted in a modest decrease in cell migration showing the dispensable nature of integrins when it comes to monocyte motility in 3D (Fig. 3A). Differentiation of the monocytes towards a highly adhesive macrophage phenotype by exposure to phorbol myristate acetate (PMA) led to substantial decrease in migration in the collagen-alginate, consistent with the known adhesion-dependence migration of macrophages (2) (Fig. S4).

Given the independence of migration on β1 and β2 integrin, as well as DDR1, we sought to further investigate the role of adhesions in monocyte migration. To this end, we performed cell migration studies in pure alginate hydrogels that did not contain any cell-adhesion ligands (Fig. 3D). Monocytes encapsulated in the collagen free viscoelastic matrices had similar morphologies to those in the collagen-1 rich IPN matrices (Fig. 3D). Cells migrated robustly in the pure alginate gels, with a slight increase in speed for slow relaxing alginate without collagen (Fig. 3E). Furthermore, the MSD showed similar diffusive behavior for cells encapsulated in slow relaxing viscoelastic matrices with or without collagen (Fig. 3F). But there was an increase in MSD diffusive behavior and directionality for cells in fast relaxing matrix without collagen (Fig. 3F). Morphological and migration similarity with and without adhesive cues suggest similarity in the mode of migration in the different matrices. These data demonstrate that cell-matrix adhesion is not required for monocyte migration. Together, these results confirm cell migration in monocytes to be amoeboid and show that adhesion to the matrix is dispensable.

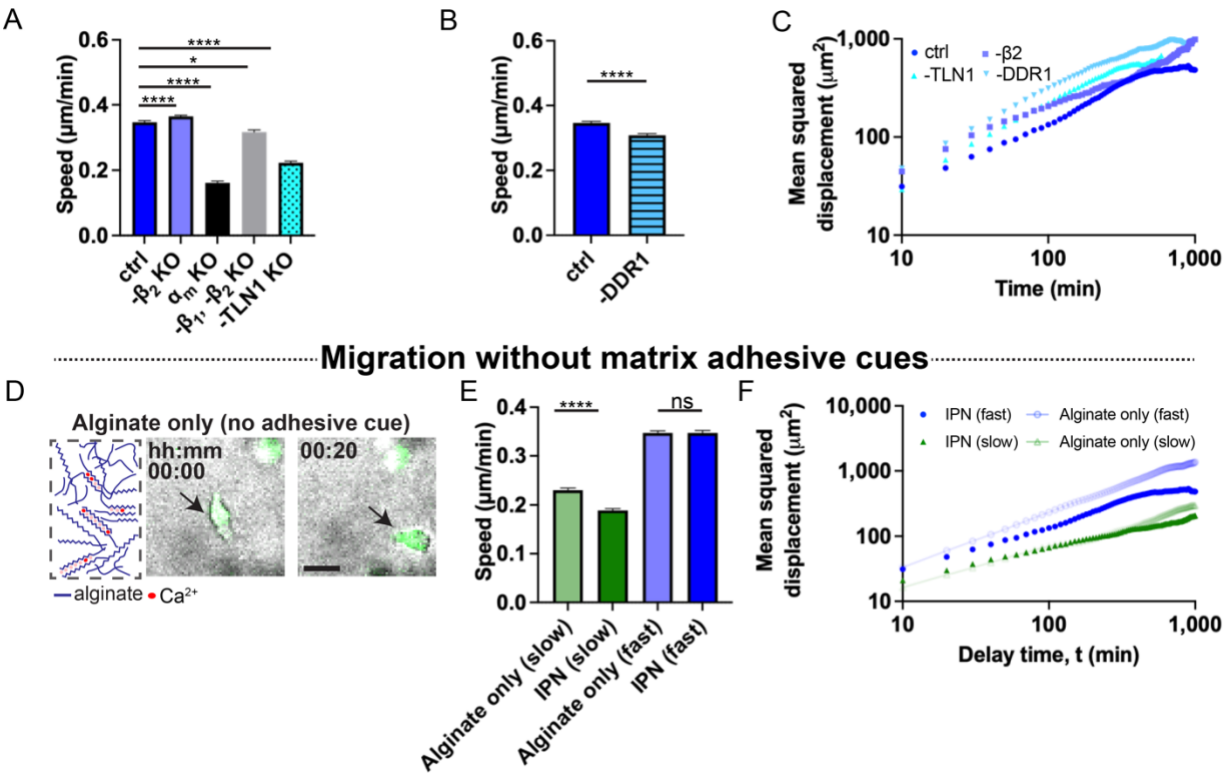

Fig. 3 Cells migrate in the collagen-alginate IPNs with amoeboid-like morphologies in an adhesion-dispensable manner. (A,B,C) CRISPR/Cas9 mediated knockout of α_M or talin-1 decreased migration but inhibition of DDR1 or β_2-integrin knockout led to no change or a slight increase in migration speed and MSD. (D) Schematic of alginate matrix without collagen adhesive cue. Typical morphology of a cell migrating in alginate viscoelastic matrix (no collagen) indicated by black arrows. Scale bar: 20 μm. (E) Cell migration speed increases for slow relaxing viscoelastic matrix without collagen compared to the IPN matrix with collagen. Migration speeds are similar for fast relaxing matrix with or without collagen adhesions. (F) Cells display similar MSD profile with or without collagen, indicating similar diffusive behavior. (A) For ctrl, -β_2 KO, and -TLN1 n > 2,102 ; N > 2 biological replicates. For -α_M KO, and -β_1, -β_2 KO n > 736 ; N = 1 biological replicate. Kruskal-Wallis test with Dunn's multiple comparisons: * p = 0.0151, **** p < 0.0001. (B) n > 2,287 for each condition; N > 2 biological replicates. (C) n > 60 for each condition; N = 1 biological replicate. (E) n > 1,606 for each condition; N > 2 biological replicates. (F) n > 145 for each condition; N = 1 biological replicate. (B,E), Kolmogorov-Smirnov: ns p = 0.1096, **** p < 0.0001.

Monocyte migration requires actin polymerization and myosin contractility

We then investigated the role of actin polymerization, myosin-mediated contractility, and the Rho pathway in mediating monocyte migration, given the known importance of the cytoskeletal machinery in driving cell migration. Actin puncta were observed at the rear of cells (Fig. 4A). The puncta remained localized at the rear of migrating cells but were uniformly distributed around the cortex of non-migrating cells (Fig. 4A). Furthermore, immunofluorescence staining revealed activated myosin staining to be somewhat diffuse throughout the cell, indicating that cell-contractility throughout the cell was not localized to any specific regions (Fig. 4B, left). In contrast, WASP, an actin nucleation promotion factor that promotes growth of a dendritic actin network through the Arp2/3 complex, was found to be localized at the leading edge of the cell, being opposite to the actin puncta at the rear of the cell (Fig. 4B, right). Therefore, these data suggest actin polymerization

mediated by WASP and the Arp2/3 complex to occur at the leading edge of the migrating cell, with dense actin puncta at the rear.

Next, actin polymerization, myosin activity, and Rho-mediated contractility were perturbed using pharmacological inhibition to determine their respective roles in cell migration and directionality of migration (Figs. 4C,D). Inhibition of actin polymerization or the Arp2/3 complex, known to drive dendritic actin networks growth, led to reduced migration speed, indicating that dendritic actin network growth at the leading edge is critical for cell migration. Similarly, inhibition of myosin light chain kinase (MLCK), an activator of myosin, potently diminished cell migration speed, indicating the role of actomyosin contractility in driving cell migration. Surprisingly, inhibition of Rho-mediated contractility through inhibition of ROCK, led to a slight increase in migration speed, contrasting the results from previous studies of amoeboid migration(14, 29). Relatedly, strong colocalization of actin and myosin was not observed as has previously been described for amoeboid migration(14, 30). Together, these findings indicate that monocytes utilize actin polymerization and myosin contractility to migrate through 3D matrices, but that the dependence on myosin contractility might be distinct from that of canonical amoeboid migration.

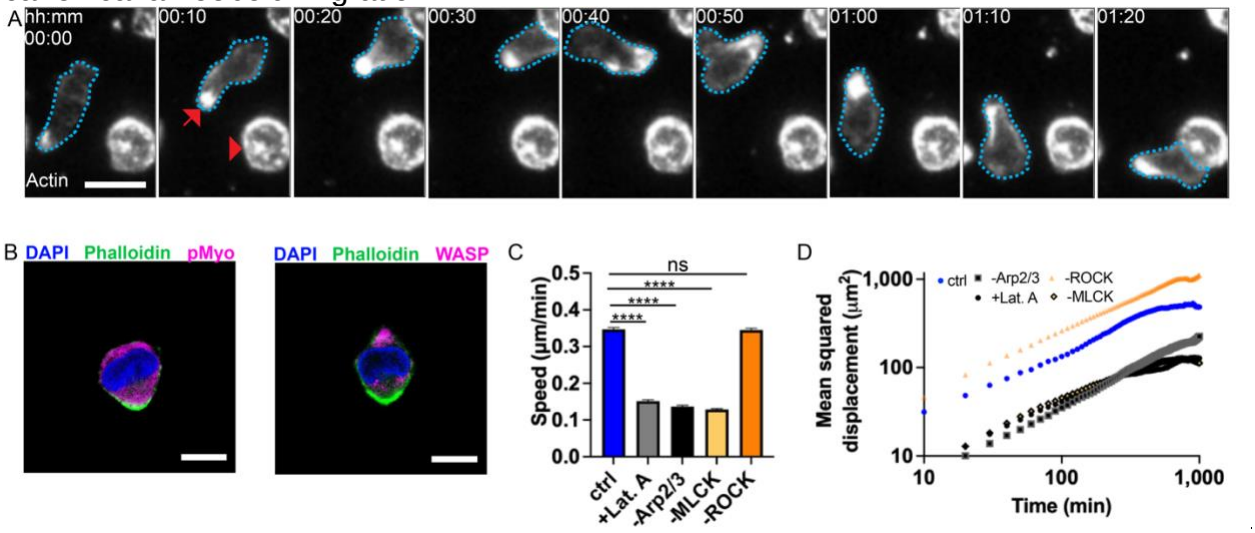

Fig. 4 Monocyte migration is dependent on actin polymerization but not Rho-mediated contractility. (A) Actin is localized at rear of migrating cell (red arrow) but uniformly distributed around cell perimeter of a non-migrating cell (arrowhead). Scale bar: 20 μm. (B) Immunofluorescence image of representative cell showing DAPI and phosphorylated myosin II. Dendritic actin nucleator (WASP) and actin filaments (phalloidin) are localized at cell front and rear respectively. Scale bar: 10 μm. (C) Inhibition of actin polymerization, decreased cell migration speed but myosin inhibition either increased or decreased migration. (D) Actin inhibition and MLCK inhibition decreased MSD indicating reduced diffusive behavior of cells whereas ROCK inhibition had the opposite effect compared to the control. (C) n > 1,351 for each condition; N > 2 biological replicates. Kruskal-Wallis test with Dunn's multiple comparisons: ns $p = 0.1496$, **** $p < 0.0001$. (D) n > 139 for each condition; N =1 biological replicate.

Actin polymerization generates protrusive forces to drive monocyte migration

The distinct localization of actin at the cell rear and front, and absence of strong colocalization with phosphorylated myosin suggested that cells might utilize actin polymerization to generate pushing forces that open up migration paths in the confining matrices (Figs. 4A,B). To investigate this, we analyzed matrix deformation as the

contractile, tangential, or protrusive nature of cell generated forces can provide additional insights into the mechanism of migration. Three-dimensional ECM deformation field around a single cell showed protrusive deformations at the leading-edge during migration (Fig. 5A). To reduce the computational requirements, we measured ECM deformation in a single optical plane of migrating monocytes and generated an average map of ECM deformations associated with cell migration and added an overlay of a representative cell shape (Figs. 5B-C). These analyses confirmed the 3D observation of cells applying pushing forces on the matrix at the leading edge, with cells pushing off of their rear and, to some extent, their sides to balance forces. Furthermore, live imaging of phalloidin demonstrated that actin filament puncta was located exclusively at the trailing edge (Fig. 4A, red arrow). Importantly, migrating cells also generated micron-sized channels in their wake, highlighting that the observed mode of migration generates migration paths in the confining matrices (Fig. 5D).

Taken together, these findings suggest a new mode of migration in monocytes (Fig. 5E). In this mode, actin polymerization generates protrusive forces at the leading and trailing edge. Divergence of stresses at the leading edge could act to rupture the IPN matrix to create micron-size channels in otherwise physically confining matrix for the monocytes to migrate through. Myosin contractility drives flow of the newly polymerized actin at the leading edge towards the rear of the cell. Cells push off their rear edge, or in some cases potentially the sides, to generate forward movement analogous to a rock climber moving up a vertical crevasse.

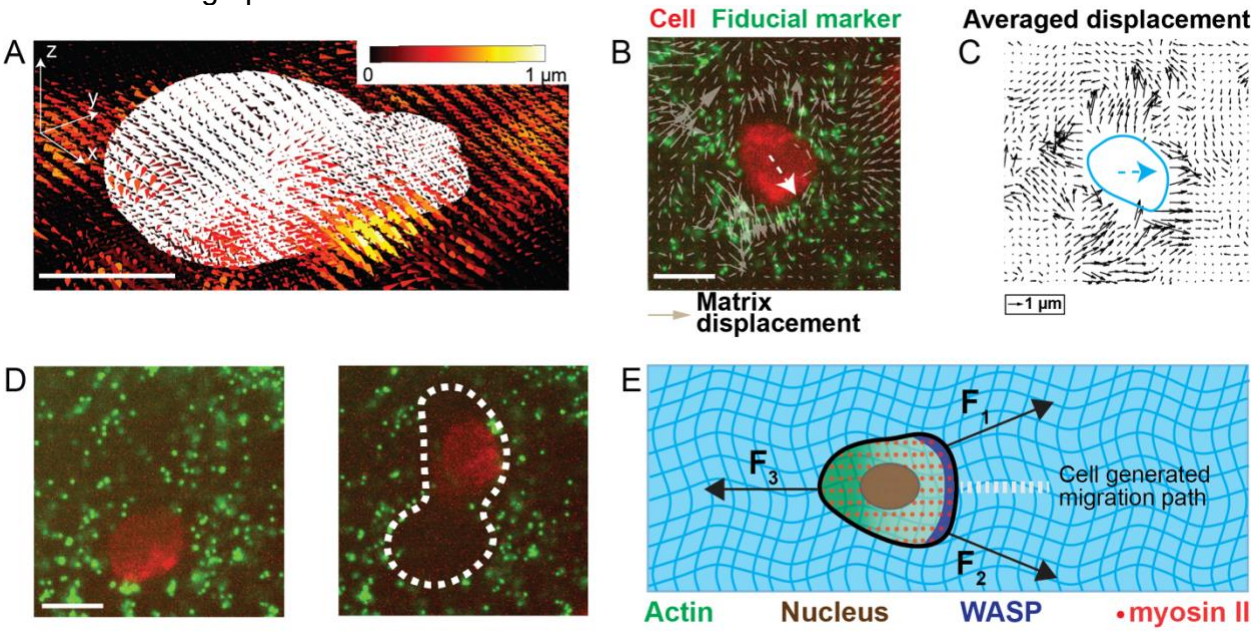

Fig. 5 Monocytes generate protrusive forces during migration through the IPN matrix. (A) Three-dimensional deformation field around a monocyte. Direction of cones represent the direction of the deformation field. Scale bar: 5 µm. (B) Confocal images of fluorescent beads (green) and a monocyte (red). Grey arrows represent ECM deformations generated during migration. White arrow (dotted): direction of migration. (C) Deformation field of ECM induced by migrating monocytes, averaged over 14 cells. Cyan arrow indicates monocyte direction of migration, cyan outline indicates cell outline, and black arrows indicate deformation field. (D) Cells open micron-sized channels to migrate. Fluorescent beads (green), and a monocyte (red) are shown 90 min apart. Dotted line (white) indicates the channel created by the monocyte. (E) Proposed model of migration. WASP mediated polymerization generates force to push matrix at the cell front, create a channel for migration while cells push off the back by using filamentous actin polymerization at cell rear

as cell migrates from left to right. (B,D) Scale bar: 10 μm. (D) 2 h (left) and 3.5 h (right) after encapsulation of monocytes in IPNs.

Discussion

We studied three-dimensional migration of monocytes in viscoelastic collagen-alginate IPNs. Increased stiffness and faster stress relaxation independently enhance monocyte migration. Monocytes migrate using amoeboid-like morphologies and depend on myosin contractility. However, myosin was diffuse throughout the cell and strong colocalization of myosin with actin was not observed as has been previously described for amoeboid migration(14). Actin polymerization at the leading edge generates pushing forces on the matrix, which opens a migration path, while myosin contractility acts throughout the cell. Together, these results describe a previously undescribed mode of monocyte migration whereby monocytes generate actin mediated protrusive forces at the leading edge to open a path to migrate in confining matrices in 3D.

We developed collagen-alginate IPNs to model the viscoelastic type-1 collagen rich stroma, and capture changes in mechanics associated with cancer progression. Prior work suggest that tissues become stiffer under some pathological conditions. However, recent findings demonstrated that alterations in tissue viscoelasticity are a feature of aberrant tissues(4, 9). Thus, the collagen-alginate IPNs were developed, in which stiffness and stress relaxation (viscoelasticity) were independently tunable, while maintaining a similar type-1 collagen rich architecture. We note that previous studies developed tunable type-1 stromal-matrix mimics using a macromolecular crowding agent (polyethylene glycol) to modulate the network architecture and mechanics of type-1 collagen gels, or click chemistry to covalently crosslink the alginate network in collagen-alginate IPNs, and thereby reduce the stress relaxation rate(24, 31). The approach described here is distinct as neither a crowding agent nor covalent bonds are involved, with IPN stiffness increased by adding more calcium ionic crosslinker and stress relaxation enhanced by lowering the molecular weight of the alginate. Thus, matrix stiffnesses from 1kPa to 2.5kPa and stress relaxation times from ~100 s to ~2,000 s were achieved, values all within physiologically relevant ranges(23).

Here we find that monocytes migrate through the collagen-rich matrices using a novel amoeboid mode of migration. Cells typically migrate in three dimensions utilizing mesenchymal or amoeboid modes of migration. Mesenchymal modes of migration typically involve spread cell morphologies, protrusions, and involve secretion of proteases combined with contractile forces at the protrusive front to generate a path for migration in confining matrices. Further, mesenchymal migration relies on strong cell-matrix adhesion while amoeboid migration uses weak adhesions. 3D migration of monocytes involved rounded or ellipsoidal morphologies and did not rely on strong adhesions, suggesting the migration mode to be more amoeboid in nature. However, there were some key distinctions with known modes of amoeboid migration. For example, Rho-mediated contractility is thought to be important for squeezing the nucleus during amoeboid migration through confining spaces, whereas monocyte 3D migration in the collagen-alginate IPNs did not require Rho activity.

In particular, our 3D migration studies tested the ability of monocytes to generate migration path, an ability which is often not assessed in other assays. Cells were embedded in three-dimensional IPN matrices that are nanoporous, therefore requiring

cells to generate micron-sized openings to migrate through. Thus, to migrate, encapsulated cells must either degrade the matrix or use mechanical force to deform or remodel the matrix. This contrasts several recent studies that monitor cell migration through microchannels in microfluidic devices, geometries where the migration path is pre-existing, or type-1 collagen matrices with sufficiently large pore sizes(32). It is likely that monocytes in vivo do not always have pre-existing paths to migrate through, as the stromal matrix is continuously being remodeled and maintained by fibroblasts, and that some dense stromal matrices they encounter exhibit pore sizes on the nanometer scale, suggesting the physiological relevance of migration path finding. As the IPNs used here contain a nanoporous alginate mesh, and as alginate is not susceptible to degradation by mammalian proteases, the robust 3D migration of the monocytes in the alginate-collagen IPNs occurs independent of proteases. This indicates that monocytes use mechanical forces to mechanically deform and remodel the matrix and generate a migration path, similar to recent observations with cancer cells and mesenchymal stem cells(26, 33). However, cancer cells were found to utilize invadopodial protrusions to generate a migration path while mesenchymal stem cells utilize a nuclear piston. Monocytes instead generate substantial protrusive forces using actin polymerization at a lamellipodia-like leading edge, and divergence of the stresses due to curvature, could act to rupture the matrix and create a migration path. This highlights a mechanism of migration path generation in confining matrices that enable cell migration.

Furthermore, the finding that monocytes possess the ability to migrate independent of adhesions is consistent with migration studies of other immune cells, though the specific nature of the cell-matrix interactions occurring during migration may be unique. Previous studies demonstrated that T-cells, macrophages, and neutrophils can migrate without adhesions in microfluidic channels with serrated edges or when confined between two macroscopic gels or between glass slides (15, 32, 34, 35). Integrin-independent migration of dendritic cells through collagen and fibrin matrix has also been reported(14). Furthermore, dendritic cells migrate in an adhesion-independent manner using protrusive actin flowing at the leading edge, similar to monocytes, but require large pore sizes and Rho-mediated contractility(14). Here, we show that monocytes migrate with similar characteristics in non-adhesive (alginate only), viscoelastic matrices as they do in collagen-rich matrices but contrary to most other immune cells do not require Rho-mediated forces to move. T-cells also can migrate in an amoeboid, adhesion-independent manner using topographical features of the matrix, and the effective friction these features generate on the sides of the cell, to propel cells forward(32). Notably, this mode of migration would result in matrix traction strains parallel to the cell body along the sides, a feature that was not consistently found with monocytes. Monocytes instead mostly typically push off their trailing edge. α_M and talin-1 perturbation led to a significant decrease in cell migration whereas β_1, β_2, and collagen receptor perturbation (DDR1) only had a moderate impact. These data suggest that monocytes migration in nanoporous matrices is primarily mediated by protrusive forces generated at the leading edge by polymerization of a dendritic actin network, actin flow to the rear of the cell, and cells pushing off their very back. Though in some cases, it is possible that friction mediated by membrane surface proteins and low affinity adhesions could contribute.

Changes in extracellular matrix (ECM) stiffness and viscoelasticity are associated with pathological conditions. In addition, mounting evidence implicates migration and

accumulation of monocytes and macrophages in disease progression. However, the potential role of ECM changes on monocyte 3D migration has not been reported. Previous work investigated the role of biochemical cues on monocyte/macrophage migration. This study raises the possibility that biophysical cues, enhanced ECM stress relaxation, promote monocyte recruitment and migration. However, monocytes could become less migratory as they differentiate into more adhesive macrophage phenotypes. Differences in migration behavior suggests that different molecular targets will likely need to be considered depending on the whether the therapeutic goal is monocyte-depletion or macrophage-depletion. More broadly, our material system provides a platform to study the role of viscoelasticity on migration of normal leukocytes and diseased leukocytes such as those with Leukocyte Adhesion Deficiency-1. Taken together, our data raises the possibility that ECM stiffness and viscoelasticity could determine immune cell recruitment and ultimately shape the immune response under normal and pathological conditions.

Materials and Methods

U937 cell culture, reagents primary human cells, and generation of cell lines.
U937 cells were maintained in suspension culture in RPMI media containing 2mM glutamine (Thermo Fisher) supplemented with 10% fetal bovine serum (FBS) (Hyclone), and 1% Penicillin/Streptomycin (Life Technologies). Cells were cultured in a standard humidified incubator at 37 °C in a 5% CO_2 atmosphere. Cells were maintained at sub-confluency and passaged every 2-3 days. To generate frozen aliquots, cells were pelleted by centrifugation (150g, 5min, room temperature), suspended in 90% FBS and 10% dimethylsulfoxide (DMSO, Tocris Bioscience), and frozen in cell-freezing containers at −80°C overnight before transfer to liquid nitrogen for long-term storage. Primary human monocytes were isolated from Leukopak following manufacturer protocols for the EasyEight separation magnet (EasySep™ human CD14 positive selection kit II, STEMCELL™ technologies). The generation of U937 CRISPR KO cell lines were described previously (36, 37). Briefly, 10-sgRNA-per-gene CRISPR/Cas9 deletion library were synthesized, cloned, and infected into Cas9-expressing U937 cells. ~300 million U937 cells stably expressing SFFV-Cas9-BFP were infected with the ten-guide-per-gene genome-wide sgRNA library at a multiplicity of infection <1. Puromycin selection (1 μg ml^{-1}) was applied to cells for 5 d. Puromycin was then removed and cells were resuspended in normal growth media (no puromycin). Flow cytometry was used to confirm sgRNA infection as >90% of cells were mCherry-positive. U937 KO lines were stored in liquid nitrogen.

Alginate preparation. Low molecular weight (MW) ultra-pure sodium alginate (Provona UP VLVG, NovaMatrix) was used for fast-relaxing substrates, with MW of <75 kDa, according to the manufacturer. Sodium alginate rich in guluronic acid blocks and with a high-MW (FMC Biopolymer, Protanal LF 20/40, High-MW, 280 kDa) was prepared for slow-relaxing substrates. Alginate was dialyzed against deionized water for 3–4 days (MW cutoff of 3,500 Da), treated with activated charcoal, sterile-filtered, lyophilized, and then reconstituted to 3.5 wt% in serum-free Dulbecco's modified Eagle's medium (DMEM, Gibco). The use of low/high molecular weight alginate resulted in fast/slow-relaxing IPNs.

Mechanical characterization of IPNs. IPNs were characterized as previously described(38). Briefly, rheology testing was done with a stress-controlled AR2000EX rheometer (TA instruments). IPNs for rheology testing were deposited directly onto the bottom Peltier plate. A 25 mm flat plate was then slowly lowered to contact the gel, forming a 25 mm disk gel. Mineral oil (Sigma) was applied to the edges of the gel to prevent dehydration. For modulus measurement, a time sweep was performed at 1 rad/s, 37 °C, and 1% strain for 3 h after which the storage and loss moduli had equilibrated. Young's modulus (E) was calculated, assuming a Poisson's ratio (v) of 0.5, from the equation:

$$E = 2(1+ v)G^*, \quad (1)$$

where complex modulus, G*, was calculated from the measured storage (G') and loss moduli (G'') using:

$$G^* = (G'^2 + G''^2)^{1/2}. \quad (2)$$

For stress relaxation experiments, the time sweep was followed by applying a constant strain of 5% to the gel, at 37 °C, and the resulting stress was recorded over the course of 3 h. For time-dependent measurements, the time sweep was followed by a creep-recovery test where a 100 Pa stress was applied to the gel and the resulting strain was measured over 1 h. The sample was then unloaded (0 Pa) and the strain was measured over an additional 2 h. The stress relaxation and creep-recovery results establish that the gels behave like viscoelastic solids.

Hydrogel formation, cell encapsulation and monocyte differentiation. For each viscoelastic gel, alginate was delivered to a 1.5 mL eppendorf tube (polymers tube) at room temperature. Rat tail collagen I (Corning), was neutralized with 10X DMEM and pH adjusted to 7.4. Neutralized collaged was added to the alginate and carefully mixed 30 times with a pipette, being careful not to generate bubbles. Extra DMEM was added to ensure 4.8 mg/ml - 1.6 mg/ml alginate-collagen final gel concentration. For 3D migration assays, cells were resuspended in growth media containing octadecyl rhodamine B chloride (R18, ThermoFisher, 1:1000 dilution of 10mg/ml stock), centrifuged, and re-suspended in growth media. The concentration of cells was determined using a Vi-Cell Coulter counter (Beckman Coulter) after passing through a 40 μM filter (Fisher Scientific) to obtain single cell suspensions. ~$2x10^6$ cells were encapsulated in each gel condition. Extra DMEM was added such that all substrates had a final concentration of 4.8 mg/mL alginate and 1.6 mg/mL collagen. This was mixed 30 times with a pipette.

Next, different calcium sulfate concentrations were added to a 1 mL Luer lock syringe (Cole-Parmer), to ensure that the initial Young's modulus is kept constant for fast, and slow-relaxing substrates. The mixture of the polymers was transferred to a separate 1 mL Luer lock syringe (polymers syringe). The calcium sulfate solution was shaken to mix the calcium sulfate evenly, and it was then coupled to the polymers syringe with a female-female Luer lock (Cole-Parmer), taking care not to introduce bubbles or air in the mixture. Finally, the two solutions were rapidly mixed together with 15 pumps on the syringe handles and instantly deposited into a well in an 8-well Lab-Tek dish (Thermo Scientific). We sought to maintain similar collagen fiber architecture when IPN stiffness and viscoelasticity was tuned. The optimal conditions we found to accomplish this was initiation of IPN gelation at 22ºC for 1 h before media was added to the wells. The samples were then allowed to gel for an additional 1 h followed by transfer to 37ºC incubator to complete gelation. Media was replaced with fresh media for all gels 24 h after

encapsulation. For cell differentiation assays, 200 ng/ml Phorbol 12-myristate 13-acetate (Fisher Scientific, PMA) was added to the gel.

Inhibition studies. Pharmacological inhibitors were added to cell media 10 minutes before time-lapse microscopy experiments. The concentrations used for the inhibitors are: 2 μM Latrunculin A (Tocris Bioscience, actin polymerization inhibitor) 100 μM Y-27632 (Sigma, ROCK inhibitor) 2 μM DDR1 (Fisher Scientific, discoidin domain receptor 1 inhibitor). Time lapse images were acquired every 10 minutes for 24 hours.

Immunofluorescence for fixed cells. Cells were embedded in matrix for 24 hours. Media was then removed from the matrix and replaced with low-melting-temperature agarose to prevent matrix from floating in subsequent steps. Matrix was then washed with serum-free DMEM and then fixed with 4% paraformaldehyde in serum-free DMEM, at room temperature, for 20 min. This was followed by three washes with Phosphate Buffered Saline (PBS) for 10 min each time. IPN hydrogels were then embedded in OCT compound (optimal cutting temperature compound; Fisher Scientific) and cryo-sectioned. Cells were then permeabilized with a permeabilizing solution for 15 min and washed twice with PBS for 5 min each time. Blocking solution was added to minimize non-specific staining. After this, primary antibodies were added overnight at room temperature and subsequently washed twice with PBS. Secondary antibodies, DAPI and phalloidin, were added for 1.5 h at room temperature followed by two PBS washes. ProLong Gold antifade reagent (Life Technologies) was added just before imaging to minimize photobleaching. Images were acquired with a Leica 25X objective.

Confocal microscopy. All microscope imaging was done with a laser scanning confocal microscope (Leica SP8) fitted with temperature/incubator control, suitable for live imaging (37 °C, 5% CO_2). In live-cell time-lapse imaging, R18 membrane labeled cells were tracked with a 20X NA = 0.75 air objective for 24 hours. For live-cell time lapse imaging, 60 μm stack images were acquired every 10 minutes and imaging parameters were adjusted to minimize photobleaching and avoid cell death.

Confocal reflectance microscopy for collagen fiber characterization. Alginate-collagen matrices in 8-well Labtek chamber were mounted on a laser scanning confocal microscope (Leica SP8) equipped with a 25X NA = 0.95 water-matched objective. A single slice of the sample was excited at 488 nm and reflected light was collected using the “Reflectance” setting on the microscope. Several, randomly selected sections of the matrix were imaged. Collagen fibril length and width were analyzed using the free and publicly available CT-FIRE software (http://loci.wisc.edu/ software/ctfire)(39-41).

Imaris cell tracking algorithm. For migration studies, the centroids of R18-labeled cells were tracked using the spots detection functionality in Imaris (Bitplane). Poorly segmented cells and cell debris were excluded from the analysis and drift correction was implemented where appropriate. A custom MATLAB script was used to reconstruct cell migration trajectory.

Measuring cell-induced ECM deformations. To measure ECM mechanical deformations induced by cell forces, we seeded IPNs with fluorescent beads following established protocols(38, 42). For 3D deformation field, we employed fast-iterative digital volume correlation(43) with a subset size of 32x32x32 voxels, and spacing of 8 voxels (2.4 μm). For 2D deformations, fast-iterative digital image correlation(44) was used on confocal images of fluorescent beads with a subset size of 32x32 pixels, and spacing of 8x8 pixels (2.4 um). To average 2D deformation field across various cells, we measured the direction of velocities of the cells, and rotated the deformation field accordingly, with each cell's velocity directed in the new x-direction. This enabled us to average the ECM deformations in the direction of cell velocities.

Statistics and reproducibility. All measurements were performed on 1-3 biological replicates from separate experiments. Exact sample size and exact statistical test performed for each experiment is indicated in appropriate figure legends. Statistical analyses were performed using GraphPad Prism (La Jolla, California). For all violin plots, broken lines are median values. For scatter plots, solid lines are median values. p-values reported were corrected for multiple comparisons, where appropriate.

Data availability

All data relevant to this manuscript are available upon request.

Acknowledgments

We acknowledge members of the Chaudhuri lab for helpful discussions and Marc Levenston (Stanford University) for use of mechanical testing equipment. We thank Vivek B. Shenoy (University of Pennsylvania) for insightful discussions. We also acknowledge the Stanford Cell Sciences Imaging Facility for Imaris software access and for technical assistance with Imaris. We thank Yael Rosenberg-Hasson for performing the flow cytometry experiments at Stanford's Human Immune Monitoring Center (HIMC). K.A. acknowledges financial support from the Stanford ChEM-H Chemistry/Biology Interface Predoctoral Training Program and the National Institute of General Medical Sciences of the National Institutes of Health under Award Number T32GM120007, and a National Science Foundation Graduate Student fellowship. This work was supported by National Institutes of Health National Cancer Institute Grant (R37 CA214136) and NSF CAREER award (CMMI 1846367) for O.C.

References

1. S. M. Crusz, F. R. Balkwill, Inflammation and cancer: advances and new agents. *Nat Rev Clin Oncol* **12**, 584-596 (2015).
2. K. Cui, C. L. Ardell, N. P. Podolnikova, V. P. Yakubenko, Distinct Migratory Properties of M1, M2, and Resident Macrophages Are Regulated by alphaDbeta2 and alphaMbeta2 Integrin-Mediated Adhesion. *Front Immunol* **9**, 2650 (2018).
3. V. Cortez-Retamozo *et al.*, Angiotensin II drives the production of tumor-promoting macrophages. *Immunity* **38**, 296-308 (2013).

4. A. Rubiano *et al.*, Viscoelastic properties of human pancreatic tumors and in vitro constructs to mimic mechanical properties. *Acta Biomater* **67**, 331-340 (2018).
5. R. Sinkus *et al.*, Viscoelastic shear properties of in vivo breast lesions measured by MR elastography. *Magn Reson Imaging* **23**, 159-165 (2005).
6. K. R. Levental *et al.*, Matrix crosslinking forces tumor progression by enhancing integrin signaling. *Cell* **139**, 891-906 (2009).
7. J. Y. Lee *et al.*, YAP-independent mechanotransduction drives breast cancer progression. *Nat Commun* **10**, 1848 (2019).
8. A. Nabavizadeh *et al.*, Viscoelastic biomarker for differentiation of benign and malignant breast lesion in ultra- low frequency range. *Sci Rep* **9**, 5737 (2019).
9. R. Sinkus *et al.*, MR elastography of breast lesions: understanding the solid/liquid duality can improve the specificity of contrast-enhanced MR mammography. *Magn Reson Med* **58**, 1135-1144 (2007).
10. O. Chaudhuri, J. Cooper-White, P. A. Janmey, D. J. Mooney, V. B. Shenoy, Effects of extracellular matrix viscoelasticity on cellular behaviour. *Nature* **584**, 535-546 (2020).
11. M. Egeblad, M. G. Rasch, V. M. Weaver, Dynamic interplay between the collagen scaffold and tumor evolution. *Curr Opin Cell Biol* **22**, 697-706 (2010).
12. P. Friedl, K. Wolf, Plasticity of cell migration: a multiscale tuning model. *J Cell Biol* **188**, 11-19 (2010).
13. M. F. Krummel, R. S. Friedman, J. Jacobelli, Modes and mechanisms of T cell motility: roles for confinement and Myosin-IIA. *Curr Opin Cell Biol* **30**, 9-16 (2014).
14. T. Lammermann *et al.*, Rapid leukocyte migration by integrin-independent flowing and squeezing. *Nature* **453**, 51-55 (2008).
15. J. Toyjanova, E. Flores-Cortez, J. S. Reichner, C. Franck, Matrix confinement plays a pivotal role in regulating neutrophil-generated tractions, speed, and integrin utilization. *J Biol Chem* **290**, 3752-3763 (2015).
16. B. Alonso-Latorre *et al.*, Distribution of traction forces associated with shape changes during amoeboid cell migration. *Annu Int Conf IEEE Eng Med Biol Soc* **2009**, 3346-3349 (2009).
17. E. Bastounis *et al.*, Both contractile axial and lateral traction force dynamics drive amoeboid cell motility. *J Cell Biol* **204**, 1045-1061 (2014).
18. A. K. Yip, K. H. Chiam, P. Matsudaira, Traction stress analysis and modeling reveal that amoeboid migration in confined spaces is accompanied by expansive forces and requires the structural integrity of the membrane-cortex interactions. *Integr Biol (Camb)* **7**, 1196-1211 (2015).
19. E. Bastounis *et al.*, The SCAR/WAVE complex is necessary for proper regulation of traction stresses during amoeboid motility. *Mol Biol Cell* **22**, 3995-4003 (2011).
20. C. A. Copos *et al.*, Mechanosensitive Adhesion Explains Stepping Motility in Amoeboid Cells. *Biophysical journal* **112**, 2672-2682 (2017).
21. J. Travnickova *et al.*, Macrophage morphological plasticity and migration is Rac signalling and MMP9 dependant. *Sci Rep* **11**, 10123 (2021).
22. C. Branco da Cunha *et al.*, Influence of the stiffness of three-dimensional alginate/collagen-I interpenetrating networks on fibroblast biology. *Biomaterials* **35**, 8927-8936 (2014).

23. O. Chaudhuri *et al.*, Hydrogels with tunable stress relaxation regulate stem cell fate and activity. *Nat Mater* **15**, 326-334 (2016).
24. K. H. Vining, A. Stafford, D. J. Mooney, Sequential modes of crosslinking tune viscoelasticity of cell-instructive hydrogels. *Biomaterials* **188**, 187-197 (2019).
25. S. C. Barnes *et al.*, Viscoelastic properties of human bladder tumours. *J Mech Behav Biomed Mater* **61**, 250-257 (2016).
26. K. M. Wisdom *et al.*, Matrix mechanical plasticity regulates cancer cell migration through confining microenvironments. *Nat Commun* **9**, 4144 (2018).
27. K. M. Yamada, M. Sixt, Mechanisms of 3D cell migration. *Nat Rev Mol Cell Biol* **20**, 738-752 (2019).
28. R. Z. Panni *et al.*, Agonism of CD11b reprograms innate immunity to sensitize pancreatic cancer to immunotherapies. *Sci Transl Med* **11** (2019).
29. D. L. Pages *et al.*, Cell clusters adopt a collective amoeboid mode of migration in confined nonadhesive environments. *Sci Adv* **8**, eabp8416 (2022).
30. E. e. a. Crosas-Molist, AMPK is a mechano-metabolic sensor linking cell adhesion and mitochondrial dynamics to Myosin-dependent cell migration. *Nature Communications* **14** (2023).
31. D. O. Velez *et al.*, 3D collagen architecture induces a conserved migratory and transcriptional response linked to vasculogenic mimicry. *Nat Commun* **8**, 1651 (2017).
32. A. Reversat *et al.*, Cellular locomotion using environmental topography. *Nature* **582**, 582-585 (2020).
33. H. P. Lee *et al.*, The nuclear piston activates mechanosensitive ion channels to generate cell migration paths in confining microenvironments. *Sci Adv* **7** (2021).
34. P. Friedl, K. Konstantopoulos, E. Sahai, O. Weiner, Adhesion-independent topography-based leukocyte migration. *Fac Rev* **11**, 18 (2022).
35. S. E. Malawista, A. de Boisfleury Chevance, L. A. Boxer, Random locomotion and chemotaxis of human blood polymorphonuclear leukocytes from a patient with leukocyte adhesion deficiency-1: normal displacement in close quarters via chimneying. *Cell Motil Cytoskeleton* **46**, 183-189 (2000).
36. M. S. Haney *et al.*, Identification of phagocytosis regulators using magnetic genome-wide CRISPR screens. *Nat Genet* **50**, 1716-1727 (2018).
37. R. A. Kamber *et al.*, Inter-cellular CRISPR screens reveal regulators of cancer cell phagocytosis. *Nature* **597**, 549-554 (2021).
38. K. Adebowale *et al.*, Enhanced substrate stress relaxation promotes filopodia-mediated cell migration. *Nat Mater* 10.1038/s41563-021-00981-w (2021).
39. J. S. Bredfeldt *et al.*, Automated quantification of aligned collagen for human breast carcinoma prognosis. *J Pathol Inform* **5**, 28 (2014).
40. J. S. Bredfeldt *et al.*, Computational segmentation of collagen fibers from second-harmonic generation images of breast cancer. *J Biomed Opt* **19**, 16007 (2014).
41. D. O. Velez *et al.*, 3D collagen architecture regulates cell adhesion through degradability, thereby controlling metabolic and oxidative stress. *Integr Biol (Camb)* **11**, 221-234 (2019).
42. R. Poincloux *et al.*, Contractility of the cell rear drives invasion of breast tumor cells in 3D Matrigel. *Proceedings of the National Academy of Sciences of the United States of America* **108**, 1943-1948 (2011).

43. E. T. Bar-Kochba, J.; Andrews E.; Kim K.-S.; Franck C., A Fast Iterative Digital Volume Correlation Algorithm for Large Deformations. *Experimental Mechanics* **55**, 261-274 (2014).
44. A. Saraswathibhatla, E. E. Galles, J. Notbohm, Spatiotemporal force and motion in collective cell migration. *Sci Data* **7**, 197 (2020).

765 **Supplementary Information**

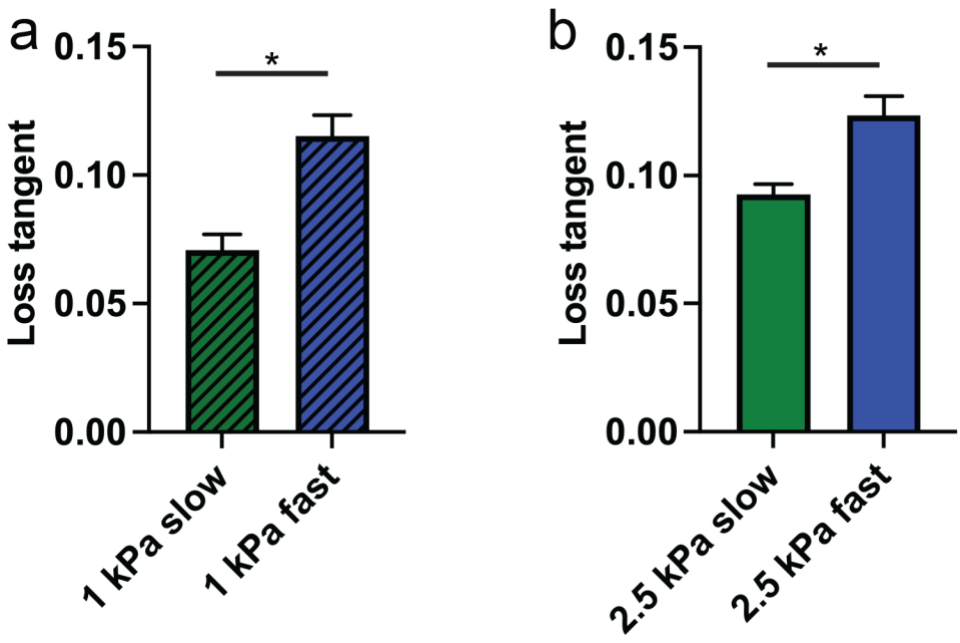

766

767 **Fig. S1** Loss tangent measurements of the different IPN formulations for slow and fast matrices.

768

769

770

771

772

773

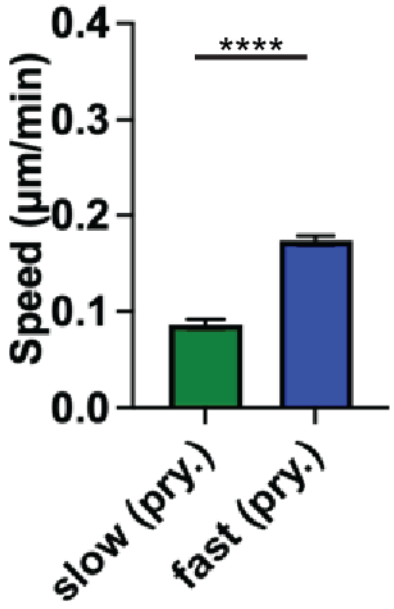

Fig. S2 Speed of migration for primary human monocytes embedded in slow and fast IPN matrices.

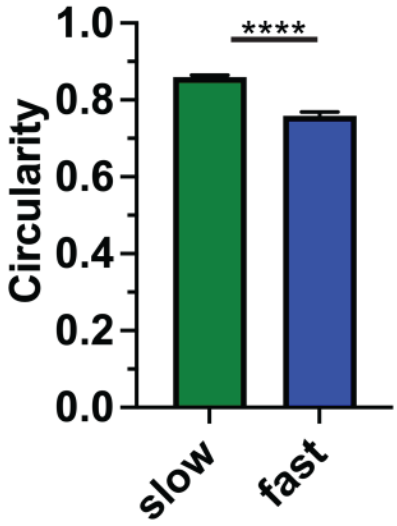

Fig. S3 Circularity for U937 human monocytes embedded in slow and fast IPN matrices.

804

805

806

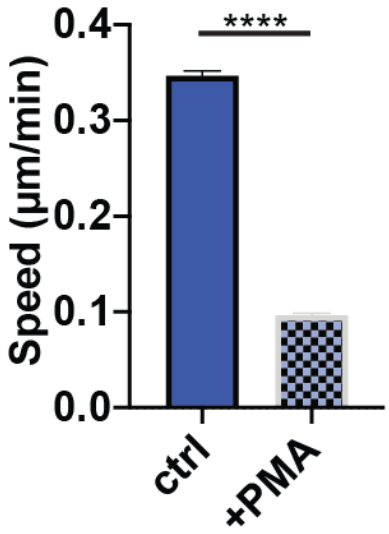

807

808 **Fig. S4** U937 migration decreases upon addition of Phorbol 12-myristate 13-acetate (PMA) to U937 cells
809 embedded in fast relaxing IPN matrix.

810

811